

COLD ROLL FORMING SIMULATION AND ORTHOGONAL EXPERIMENTAL OPTIMIZATION OF SPIRAL CORRUGATED STEEL TUBES

SIMULACIJA OBLIKOVANJA S HLADNIM VALJANJEM IN ORTOGONALNA EKSPERIMENTALNA OPTIMIZACIJA ŠPIRALNO NAGUBANIH JEKLENIH CEVI

Wan-Jun Chen, Yi-Ying Zhou, Hua-Min Liu*

College of Materials Science and Engineering, Jilin University, Changchun 130025, China;

Prejem rokopisa – received: 2024-07-02; sprejem za objavo – accepted for publication: 2024-08-27

doi:10.17222/mit.2024.1234

The cold-roll forming process is capable of producing intricate profiles, and optimizing its parameters can enhance the quality of the final product. This study focuses on analyzing the roll forming of spiral corrugated steel tubes made from galvanized sheet BGH340. The professional roll design software COPRA is utilized to design the rolls, and a three-dimensional finite-element analysis model for spiral corrugated steel tubes rolls is established. Orthogonal experiments are conducted to investigate the effects of the friction coefficient, line velocity, and rotation angle on the maximum longitudinal strain. The results indicate that increasing the friction coefficient can help reduce the strain, but may also result in defects such as scratches. Line velocity has the most significant impact on strain, with higher line velocities leading to increased strain and resulting in side wave and plate surface inequality defects. The rotation angle has a minimal influence on strain levels. The optimum contour parameters are deduced based on these findings, providing a theoretical foundation that directly contributes to improving the production efficiency and ensuring higher quality in the manufacturing of spiral corrugated steel tubes.

Keywords: cold roll forming, spiral corrugated steel tubes, finite-element analysis

S postopkom hladnega valjanja lahko izdelujemo različne profilirane izdelke. Z optimiziranjem njegovih procesnih parametrov izboljšamo tudi kvaliteto končnega izdelka. V članku avtorji opisujejo študijo, v kateri so se osredotočili na analizo hlanega valjanja špiralno nagubanih cevi, izdelanih iz galvanizirane jeklene pločvine vrste BGH340. Avtorji so uporabili profesionalno programsko orodje COPRA za oblikovanje valjev za nagubane cevi in izdelavo tridimenzionalnega (3-D) modela za analizo s pomočjo metode končnih elementov (FEM). Izvedli so ortogonalne preizkuse, s katerimi so določili vpliv koeficienta trenja, linijske hitrosti in rotacijskega kota na maksimalno deformacijo v (vzdolžni) smeri valjanja. Rezultati preizkusov so pokazali, da povečevanje koeficienta trenja lahko zmanjša deformacijo, toda tudi povzroči napake na ceveh, kot so na primer raze. Linijska hitrost ima največji vpliv. Višja hitrost povzroča večjo deformacijo, stranske valove in neenakomerno velikost napak na površini. Kot rotacije ima zanemarljiv vpliv na deformacijo. Parametre optimalne oblike profila so avtorji dobili na osnovi izvedenih preizkusov in teoretičnih modelnih analiz. S študijo so avtorji predstavili temeljne teoretične osnove, ki lahko direktno prispevajo k izboljšanju učinkovitosti proizvodnje in izdelavo bolj kvalitetnih špiralno nagubanih cevi.

Ključne besede: oblikovanje s hladnim valjanjem, špiralno nagubane cevi, analiza s pomočjo metode končnih elementov

1 INTRODUCTION

Cold-roll forming technology is an advanced, continuous, local cold-working process. It involves applying external force to metal bending areas repeatedly, causing them to bend and deform, thus producing products with predetermined shapes.¹ This technology offers advantages over traditional hot-roll forming in terms of production efficiency, energy consumption, and product quality.² Widely used as an efficient and economical forming method for producing corrugated steel pipes, cold-roll forming technology allows for a precise adjustment of the parameters in the cold-bending forming equipment, to control the bending radius, rotation angle, and length of the forming process, resulting in corrugated steel pipes of various shapes.³

Spiral corrugated steel tubes play an essential role in multiple fields due to their high strength, good flexibility, lightweight structure, rapid construction, long life, excellent ecological and environmental performance, and low comprehensive engineering costs. They are considered an ideal substitute for non-metallic pipe materials and are essential in applications such as underground drainage, urban sewage systems, highway culverts, shared utility tunnels, drilling pipes, irrigation channels, and mine escape passages.⁴⁻⁷ However, the deformation that occurs during the cold bending process is complex, influenced by material nonlinearity, geometric nonlinearity, and boundary nonlinearity. In the cold bending simulation of spiral corrugated steel tubes, accurately simulating the material behavior is crucial to ensuring the finished product's forming quality and geometric accuracy.^{8,9} Q. V. Bui explored the impact of material properties, such as yield limit and work-hardening index, on the cold-roll forming process using 3D finite-element

*Corresponding author's e-mail:
liuhm@jlu.edu.cn (Hua-Min Liu)

analysis.¹⁰ X. Chen utilized MARC software to investigate the importance of material behavior on the formation process, particularly in relation to the precise simulation and control of spiral corrugated steel tubes forming. Rotation angle, forming steps, and residual stress were found to have a substantial impact on the overall forming process. Optimizing these parameters can effectively minimize defects during the spiral corrugated steel tubes forming process, such as edge corrugation and buckling, thus improving product quality.¹¹ Shim used ABAQUS to explore the role of forming parameters in reducing the waviness of the corrugated sheet edges, which is significant for the optimization of spiral corrugated steel tubes forming.¹² Tehrani analyzed the effect of rotation angle and steps on edge buckling during cold-roll forming using ABAQUS, offering valuable insights for enhancing the spiral corrugated steel tubes forming process.¹³

This study employs a digital design approach that integrates theory and experience to facilitate the digital transformation of the spiral corrugated steel tubes roll pressing process design. We developed an optimized roll-pressing process scheme for spiral corrugated steel tubes through simulation analysis and process parameter optimization. The study investigated the main factors affecting edge wave defects in spiral corrugated steel tubes roll pressing forming, such as finite-element calculation methods, plate thickness, friction coefficient, line velocity, and rotation angle. The paper primarily focuses on conducting thorough research on the latter three aspects.

2 MATERIAL PROPERTIES AND MESH

2.1 Material characteristics

In this study we selected BGH340 galvanized sheet as the key material for our experiments, with some of its material parameters presented in **Table 1**. This material is widely used in the construction industry due to its excellent corrosion resistance, high strength, and superior rigidity, especially in applications that demand structural

integrity and durability. The BGH340 galvanized sheet, treated with hot-dip galvanizing, not only enhances its corrosion resistance but also improves the overall performance of the material, which is crucial for ensuring the quality of the forming process and the reliability of the finished product.

During numerical simulation analysis, we strictly defined and controlled the physical dimensions of the BGH340 galvanized sheet. The selected sheet has a width of 308 mm and a thickness of 1.5 mm. These dimensional parameters were carefully chosen based on typical architectural application requirements and to ensure the accuracy of the simulation. Such size specifications not only meet our experimental needs but also ensure that the simulation results are consistent with real-world production environments.¹⁴

Furthermore, we employed the continuous forming method for product modeling. This method not only simulates various aspects of the continuous forming process but also accurately reproduces the material’s behavior during forming, including stress distribution, deformation patterns, and any potential defects. Through this precise modeling approach, we can thoroughly analyze and optimize the cold-roll forming process of spiral corrugated steel tubes, thereby enhancing the quality and performance of the final product.

Table 1: Properties of the elastic stage of the material

Parameters	Units	Values
Young’s modulus (E)	GPa	210
Poisson’s ratio (ν)	–	0.3
Yield stress (σ_s)	MPa	328
Ultimate tensile strength	MPa	491
Density	Kg/m ³	7850

2.2 Mesh division

Our research utilized the mesh adaptive division function within the COPRA system to optimize mesh density in the bending areas, where plastic deformation and stress concentration are critical during the cold-roll

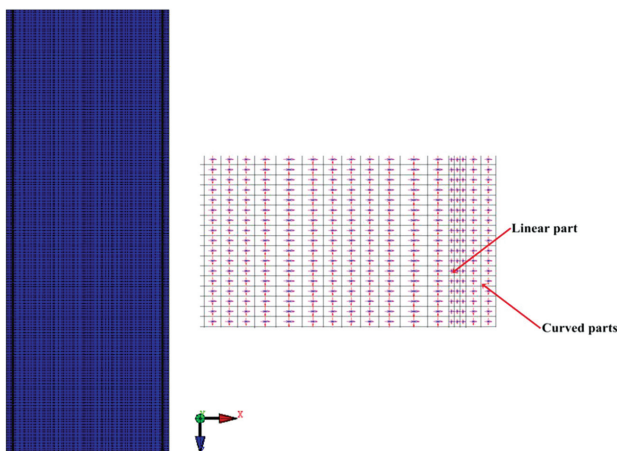


Figure 1: Billet structure diagram

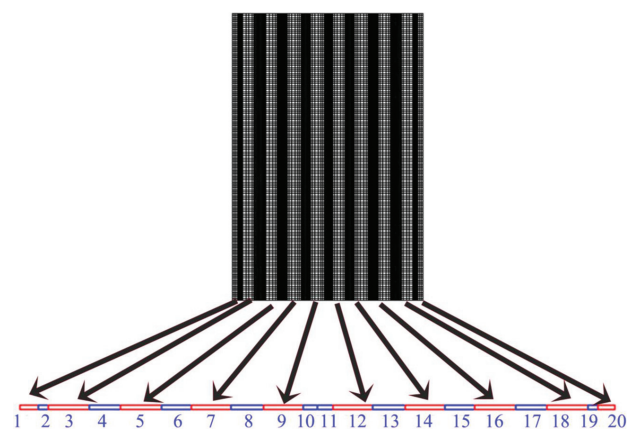


Figure 2: Blank grid division

forming process. This densification was essential to ensure accurate simulation of the deformation behavior.

We balanced computational efficiency and accuracy by implementing a mesh model with 38,871 nodes and 16,354 elements. While a denser mesh could have provided more detail, it would have greatly increased the computational costs. Conversely, a coarser mesh would have been less computationally demanding but risked losing essential details in areas with complex stress distributions.

By adopting a three-dimensional solid mesh in thickness, we maintained necessary accuracy without imposing excessive computational loads. This approach enabled us to effectively capture key physical phenomena, while ensuring the process remained computationally efficient. The layout and details of the mesh division are illustrated in **Figures 1 and 2**.

3 ESTABLISHING A FINITE-ELEMENT ANALYSIS MODEL

3.1 *Spiral corrugated steel tubes forming method*

The forming process of spiral corrugated steel tubes is a technically demanding and complex manufacturing procedure, mainly comprising four key stages: the bite-in stage, the cold-roll forming stage, the three-roll bending forming stage, and the spiral tilting stage. This series of carefully designed stages ensures the high standards of spiral corrugated steel tubes regarding shape accuracy and mechanical properties.¹⁹

During the bite-in stage, the strip is precisely introduced between the rolls. This stage aims to ensure the stability of the strip, laying the groundwork for the subsequent processing steps. At this point, the rolls provide necessary support and apply appropriate boundary constraints, ensuring that the strip is fixed in width (X-direction) and thickness (Y-direction) and maintains uniform movement in the rolling direction (Z-direction).²⁰

Then, the process enters the roll-forming stage, where the strip starts forming operations. Unlike the bite-in stage, this stage releases constraints on the thickness direction of the strip, allowing it to bend and deform freely in a lateral direction. The constraints in the rolling direction become more complex, closely related to the friction force between the rolls and the strip, often simulated precisely using numerical simulation techniques such as the User Sub-Forcedt method in MARC software.

Next is the three-roll bending forming stage, where the strip is finally bent and formed through three sets of rollers. These rollers' intricate design and arrangement directly determine the final shape and dimensional accuracy of the spiral corrugated steel tubes. In this stage, the initial gap between the first set of upper and lower rolls is 10 mm. As the plate enters the roll gap, its front end is 20 mm ahead of the central line of the upper and lower rolls, and the upper roll is pressed down to initiate the forming process.

Finally, the spiral tilting stage gradually forms the strip into a spiral shape by adjusting the rotation angle α of the three sets of rolls, as shown from **Figure 3a** and **3b**. To achieve a connection effect, a part of the front end of the plate needs to be cut off after a period. The key in this stage lies in precisely controlling the rotation angle of the rolls and the timing of cutting to ensure the accuracy of the spiral corrugated steel tubes shape and the tightness of the seam.

Throughout the forming process, precise control of various parameters and roll actions is crucial, directly impacting the quality of the final product. These meticulous operations and adjustments make spiral corrugated steel tubes precisely manufactured to meet the required physical and geometrical characteristics.

3.2. *Rolls design*

The roll pattern is a schematic cross-sectional view of the roll-forming unit during the sheet-forming process, as shown in **Figure 4**. The rolling pattern is a crucial element, depicting the cross-sectional view of the sheet in the roll-forming unit. This pattern is meticulously designed using COPRA's stick-type design module to demonstrate the sequence and process of sheet forming. The design specifies the exact steps the sheet undergoes during the forming process. In this design, we focused on some key parameters: the setback radius was set at 5 mm, the sheet thickness at 1.6 mm, and the total bite angle reached 130 degrees, with the entire process divided into four stages. The sectional hole pattern designed based on these requirements is shown in **Figure 4**.

This precise design fully considers the physical properties of the material, especially the spring-back effect. We observed that the spring-back phenomenon is minimal in the central part of the material and becomes more pronounced towards the edges. Understanding and con-

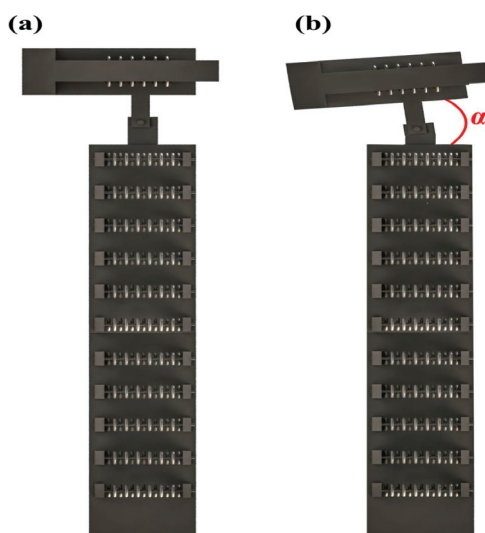


Figure 3: Spiral tilting stage: a) before spiral and b) after spiral

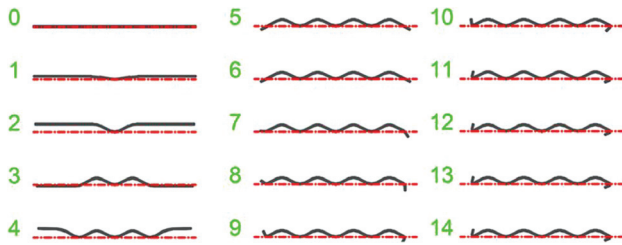


Figure 4: Flower pattern

trolling this phenomenon is crucial for optimizing the forming process.²¹

After careful planning and design, the entire forming process is completed through 14 stages, successfully forming the desired cross-sectional shape. The precise execution of this series of stages ensures that the final product’s shape meets the design requirements, while maintaining the material’s structural integrity and performance standards. Through such a refined process, we are able to produce high-quality sheets that meet stringent standards.²²

3.3 Roll optimization based on DTM analysis

In this study we utilized the Deformation Technology Module (DTM) of COPRA for an in-depth analysis. Through the DTM we conducted a detailed analysis of the pre-designed roll patterns to measure the steel strip’s strain level accurately under the given roll pattern design. As observed in the DTM analysis shown in **Figure 5a**, the longitudinal strain on the steel strip is relatively small during horizontal forming. As the depth of forming increases, the strain value correspondingly increases, which is in complete agreement with theoretical predictions.

Figure 5b shows the visual representation of the DTM simulation. In this simulation, the pass interval was set to 250 mm. The black strips in the figure represent the transition areas during the forming process. The tail end of one black strip to the tail end of the next black

strip defines the pass interval. From the figure it is clear that the length of the forming transition area is approximately one-third of the pass interval. Therefore, based on the DTM simulation, we can infer that the smooth transition area between adjacent passes is about 300 mm.

Based on suggestions from actual production feedback and to avoid affecting the adjustment of matching rolls and auxiliary mechanisms, we first conducted preliminary simulations using DTM before performing extensive simulations. The purpose of this initial simulation was to verify the correctness of the roll-pattern design. This approach not only improved the efficiency of the design but also ensured the smooth progress of the forming process, thereby enhancing the quality and consistency of the final product. Through such precise prediction and analysis, we can effectively guide and optimize the production process in the early stages.

3.4 Establishing a finite-element analysis model

In this study we used the COPRA2021 software developed by Germany’s Data M company for the precise design of the rolls. We imported the completed roll patterns into COPRA FEA for further analysis. COPRA FEA is an advanced finite-element analysis tool integrated into MARC software, particularly adept at performing complex contact analysis.^{23,24}

We fully leveraged the powerful capabilities of MARC software, especially in simulating contact processes. By integrating traditional gap friction elements, MARC can precisely simulate the contact points between the structures. Contact constraints can be applied through Lagrange multipliers or penalty function methods, accurately reflecting actual contact situations in simulations.²⁵ Additionally, MARC provides advanced contact iteration algorithms based on the direct constraint method, allowing the software to analyze the contact situations automatically between deformable bodies, between deformable and rigid bodies, and within themselves. When contact occurs, MARC constrains the mov-

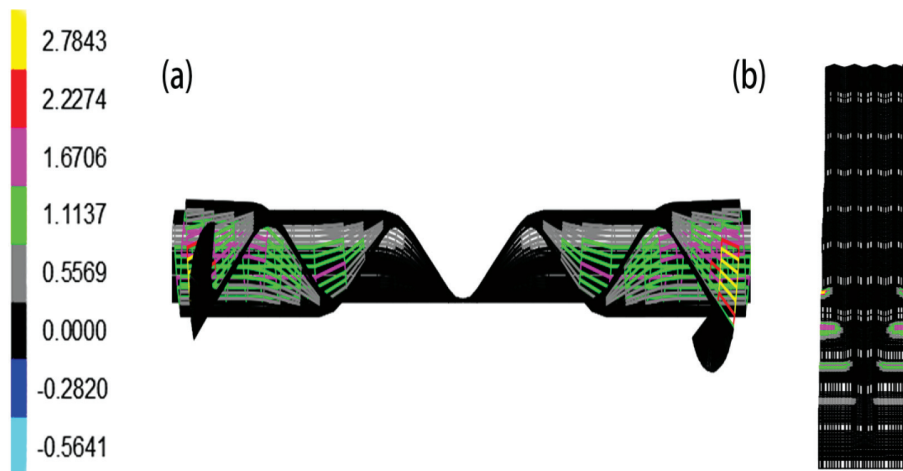


Figure 5: a) DTM analysis and b) the visual representation of the DTM

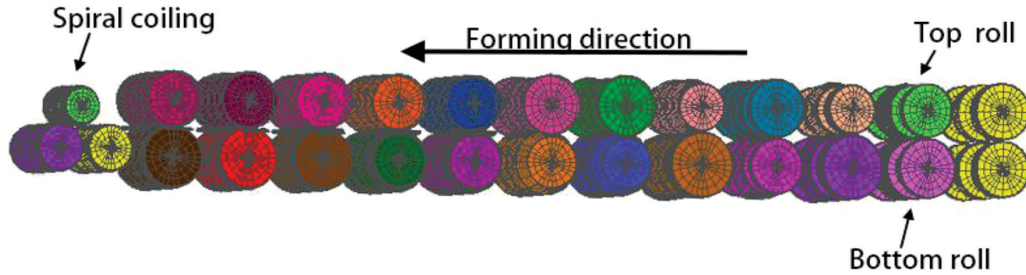


Figure 6: Assembly of cold-roll forming

ing body by applying boundary conditions, converting motion restrictions into constraints on the nodes' degrees of freedom and nodal force constraints. Unlike traditional methods, MARC does not require pre-specification of the reference elements, thus effectively handling complex situations involving large contact areas and uncertain contact regions.

To ensure the accuracy of the simulation results and their similarity to actual production, we meticulously set a series of key parameters, including sheet length, material properties, diameters of the upper and lower rolls, distance between rolls, and contact conditions. The precise setting of these parameters ensures the authenticity and reliability of the simulation results.

We performed detailed work using COPRA software to construct the geometrical model of each pass section and roll. First, we imported the profile diagram of the spiral corrugated sheet from AUTOCAD into COPRA and then generated the corresponding roll pattern based on preset parameters. After pre-optimizing the roll pattern using DTM, we obtained detailed roll diagrams for each pass section, which are crucial for optimizing and designing the entire forming process.

Finally, considering the importance of the spring-back phenomenon, we paid special attention to it in our simulations. The stick comprises 15 stations and is assembled, as shown in Figure 6. Spring back occurs due to the release of stored elastic deformation energy during unloading, which is influenced by many factors. However, the profile's material properties and bending radius are the most critical. Therefore, we carefully con-

sidered these factors in our study to ensure the accuracy and practicality of the simulation results.

4 RESULTS AND DISCUSSION

4.1 Simulation results analysis

After defining the roll pattern, we employed an innovative Deformation Technology Module (DTM) to optimize the initial design. In the roll-forming process, longitudinal strain often occurs at the edges of the sheet due to the need to cover a longer distance than the undeformed area. To effectively address this challenge, we introduced a linear method that considers the forming length.

This module integrates finite-element analysis with a wealth of experimental data. By comprehensively considering the geometric deformation and material characteristics, it accurately assesses the forming quality. This approach not only resolves potential issues in the design stage but also significantly reduces the workload required for DTM debugging. This method greatly accelerates the trial cycle for new products while reducing material costs.

The Von Mises stress calculated by Equation 1 is essential for predicting the potential yield points of the material under combined stresses. As shown in Figure 7a, stress concentrations form along the strip, corresponding to the locations with the highest Von Mises stresses, as predicted by Equation 1. Additionally, Figure 7b provides a front view illustrating how stress is distributed across

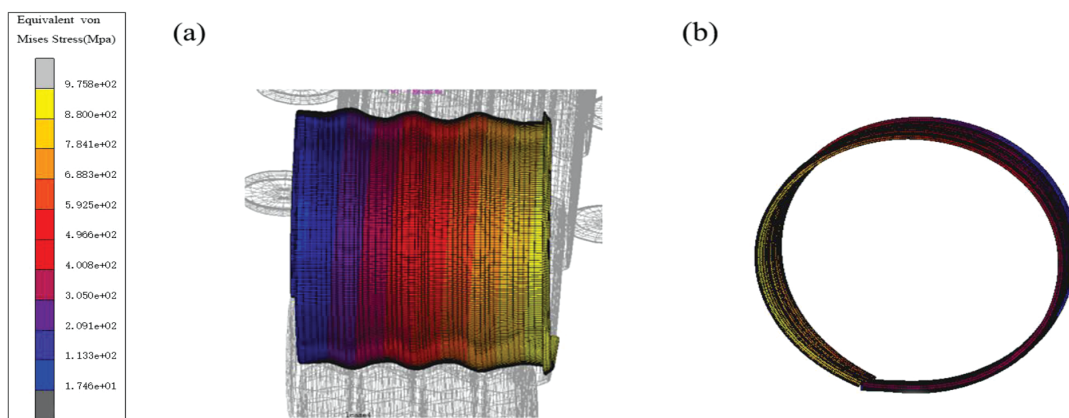


Figure 7: Variation of the equivalent von Mises stress distribution of strip: a) side view and b) front view

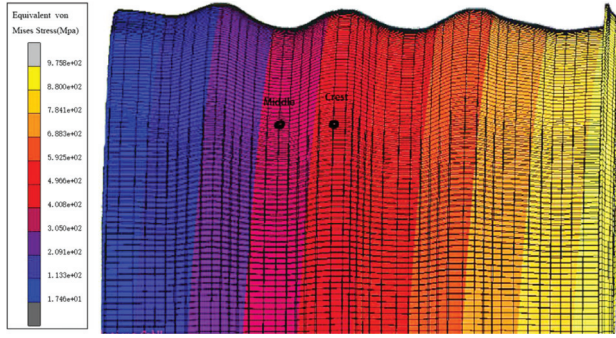


Figure 8: Measurement position

the entire width of the strip. This comprehensive visualization aids in understanding the uniformity of the stress distribution and ensures that the theoretical calculations align with practical outcomes observed in the simulations.

Equation (1) governs the calculation of the equivalent Von Mises stress:

$$\sigma = \left\{ \frac{1}{2} \left[2(\sigma_x^2 + \sigma_y^2 + \sigma_z^2) - 2(\sigma_x \sigma_y + \sigma_y \sigma_z + \sigma_z \sigma_x) + 3(T_{xy}^2 + T_{yz}^2 + T_{zx}^2) \right] \right\}^{1/2} \quad (1)$$

where σ represents the equivalent Von Mises stress, σ_x, σ_y and σ_z are the normal stresses in the $x, y,$ and z directions and T_x, T_y and T_z are the shear stresses in the $xy, yz,$ and zx planes, respectively.

The simulation results revealed the characteristics of the workpiece in the initial stages of bending deformation. In this stage, the plastic equivalent strain at the front end of the workpiece along its length is zero, while the elastic equivalent strain gradually increases. This indicates that the workpiece is still in the state of elastic deformation at this stage, without plastic deformation. As the elastic equivalent strain increases to a certain level, its rate of change tends to stabilize and maintains a relatively fixed value. At this point, the plastic equivalent strain begins to increase gradually, marking the transition of the workpiece into the plastic deformation stage. Sub-

sequently, the elastic equivalent strain slightly increases, while the plastic equivalent strain continues to rise.

When the plastic equivalent strain reaches a specific value, both elastic and plastic equivalent strains tend to stabilize, and the workpiece achieves a stable state of bending deformation. Under the deformation conditions of corrugated pipes, when the equivalent stress reaches a certain threshold, it causes plastic deformation of the material. The stress distribution is primarily concentrated at the contact points between the rolls and the strip, with higher stress near the bending area and reduced stress in the surrounding regions.

The cold-roll forming process involves significant deformation, particularly at the edges of the strip, where the complex stress state increases the likelihood of instability. To gain a better understanding of this phenomenon, we conducted a detailed analysis using specific parameters (spacing 300 mm, friction coefficient 0.05, line velocity 10 min⁻¹, rotation angle 0.05 rad), focusing on key areas such as the crests and middle of the strip.

Figure 8 identifies the measurement positions along the strip and visually depicts the stress distribution through a color gradient. This figure clearly shows that stress is concentrated at the crests, with higher levels indicated by warmer colors. This distribution suggests that these areas are more susceptible to deformation and potential defects.

Figure 9 provides a deeper analysis of these critical points. Figure 9a illustrates the strain curves for different positions along the strip edge. It is evident that strain is highest at the crests, where the material experiences greater deformation. This increased strain correlates directly with the stress concentrations observed in Figure 8.

In Figure 9b, stress curves for same positions are presented. The data confirms that stress peaks at crests with a sharp rise as the material undergoes bending. This stress increase continues until the material reaches its maximum strain capacity, after which it levels off, indicating a point of material stability or potential failure.

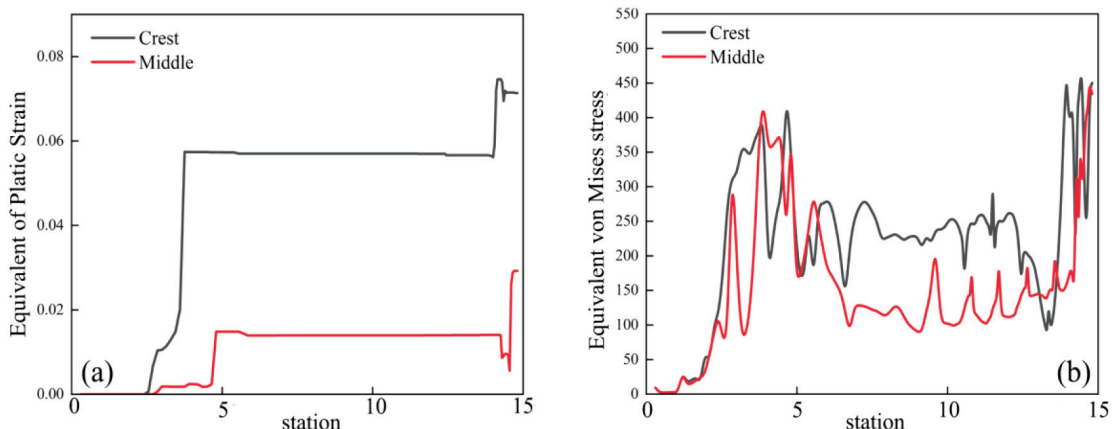


Figure 9: a) Strain and b) stress curves at different positions of the strip edge

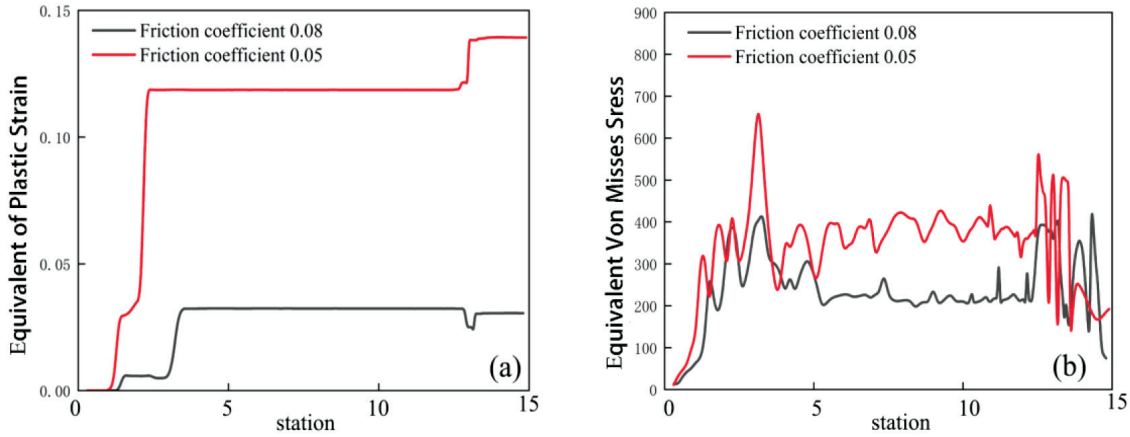


Figure 10: a) Strain and b) stress curves for two different friction coefficients

The combined analysis from **Figures 8 and 9** reveals that the crests are the most critical areas during the bending process, where the interplay between stress and strain is most pronounced. This understanding is crucial for optimizing the bending process to reduce the risk of defects, especially in high-stress, high-strain zones.

4.2. Friction coefficient

To further investigate the influence of the friction coefficient on the roll-forming process, we conducted a simulation study with the following parameters: a line velocity of 10 mm/s, a rotation angle of 0.05 rad, and two different friction coefficients (0.05 and 0.08). **Figure 10** clearly illustrates the distribution of equivalent strain and stress in the material under varying friction conditions. The findings indicate that distinct sections of the plate exhibit diverse levels of friction, resulting in varying maximum equivalent strain values. It is evident that consistent friction coefficients are maintained across different plate sections due to increased resistance between the roll and plate caused by higher friction coefficients, which hinders smooth flow within the roll. Moreover, higher friction coefficients correspond to lower values of the equivalent plastic stress, effectively reduc-

ing the rotation angle rebound after elastic recovery occurs when exiting the roll. This finding is significant as it helps mitigate the rebound by increasing the forming force during production for materials prone to substantial elastic recovery; thus lubrication may be omitted in favor of dry friction production in such cases. Additionally, moderate increases in roll friction can minimize the rotation angle rebound and ensure product quality.

4.3 Line Velocity

In order to investigate the influence of line velocity on the roll-forming process, specific parameters were set in our simulation experiments. The line velocity was adjusted to 10 min⁻¹ and 3 min⁻¹, with the rotation angle set at 0.05 rad and the friction coefficient fixed at 0.05. **Figure 11** illustrates the distribution of equivalent strain and stress under these conditions. It is evident from the figure that the two patterns of change are similar. As shown in the figure, equivalent stress generally increases with the line velocity, but during the molding stage, stress at the Angle frame increases with a higher line velocity. **Figure 11** indicates that the line velocity tends to promote strain. In summary, it is clear that a higher line velocity generally increases the plate stress and strain,

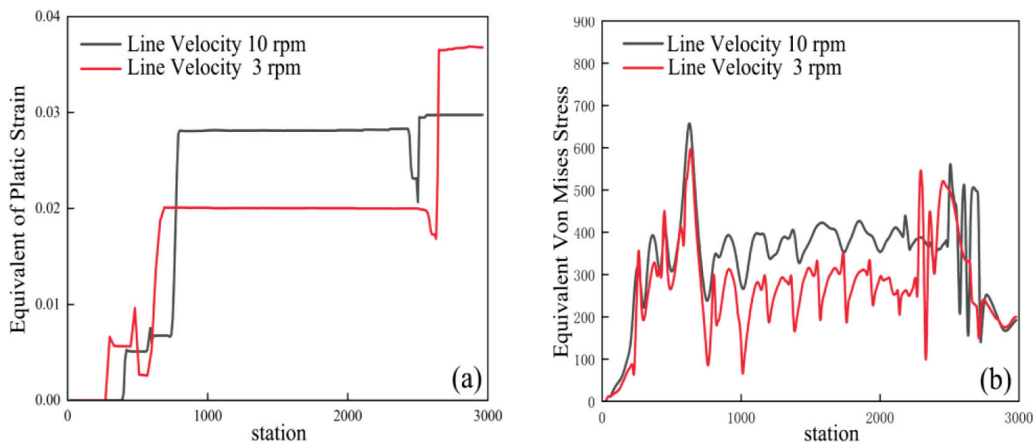


Figure 11: a) Strain and b) stress curves for two different line Velocity

which is not conducive to effective molding. Additionally, different design angles exhibit similar changes under n identical line velocity.

4.4 Rotation angle

To understand the impact of rotation angle on the roll-forming effect, we set the following parameters in our simulation: a line velocity of 10 min⁻¹, with rotation angles set at 0.05 rad and 0.07 rad, while maintaining the friction coefficient at 0.05. In **Figure 12** we displayed the distribution of equivalent strain and stress under these two rotation angles.

The simulation results show that at the edge level, the longitudinal strain experiences slight fluctuations as the rotation angle increases. Especially at larger rotation angles, with increased depth, there is a sudden change in the edge strains. This indicates that the impact of rotation angle on the edge strain varies with different forming stages. However, this impact is relatively minor overall, suggesting that the rotation angle does not significantly influence the longitudinal strain at the edges.

This finding is significant for optimizing the roll-forming process. While the rotation angle does affect edge strain to some extent, its rotation angle of impact is limited. This means that when setting the forming parameters, the rotation angle can be adjusted within a certain range, without greatly affecting the forming quality. This offers greater flexibility in designing and adjusting the roll-forming process.

4.5 Analysis of orthogonal experiment results

Using the L8(2⁷) orthogonal experimental design, this study analyzed two factors at three levels and conducted nine experiments. The relevant parameters and their levels are detailed in **Table 2**. We calculated the maximum longitudinal strain for each experiment and summarized the results in **Table 3**. **Table 3** shows the orthogonal array and the maximum strain values and in-

cludes the signal-to-noise ratio, which is a key indicator for evaluating the experimental results.

Subsequently, we conducted an in-depth analysis of the data in **Table 3** using the mean-analysis method. As the goal of this study is to minimize the maximum longitudinal strain in each process, we used the ‘smaller-the-better’ characteristic formula to calculate the average signal-to-noise ratio for each level of each parameter in the eight experiments. A higher signal-to-noise ratio indicates minor strain and, thus, better-forming quality. These analysis results are detailed in **Figure 12**.

Additionally, we performed a range analysis, and the results are presented in **Table 4**. This analysis shows each parameter’s range R (as shown in **Table 4**) at different levels. A parameter with a large R value indicates a significant impact on the experimental indicators; conversely, a small R value implies a lesser impact. This range analysis helps us better understand the degree of influence of each parameter on the final results, thus providing an important basis for further optimization of the forming process.

Equations (2) and (3) are used to calculate the S/N ratios, which quantify the relationship between the input parameters and the resulting strain. Equation (2) is used to determine the S/N ratio for each individual experiment, highlighting the impact of each experimental run on the overall process stability. Subsequently, Equation (3) aggregates these individual S/N ratios to assess the overall influence of each parameter.

$$(S/N)_i = -10 \times \lg_{10} \left(\frac{1}{n} \sum_{i=1}^n y_i^2 \right) \tag{2}$$

$$(S/N)_{F_j} = \sum_1^m \frac{(S/N)_i}{m} \tag{3}$$

where y_i is the calculated value for each experiment, n is the number of repeated experiments, and $(S/N)_i$ is the signal-to-noise ratio. $(S/N)_{F_j}$ represents the level value of parameter F ; m is the number of experiments in which the level value of parameter F participates; and $(S/N)_i$ is the signal-to-noise ratio of F_j .

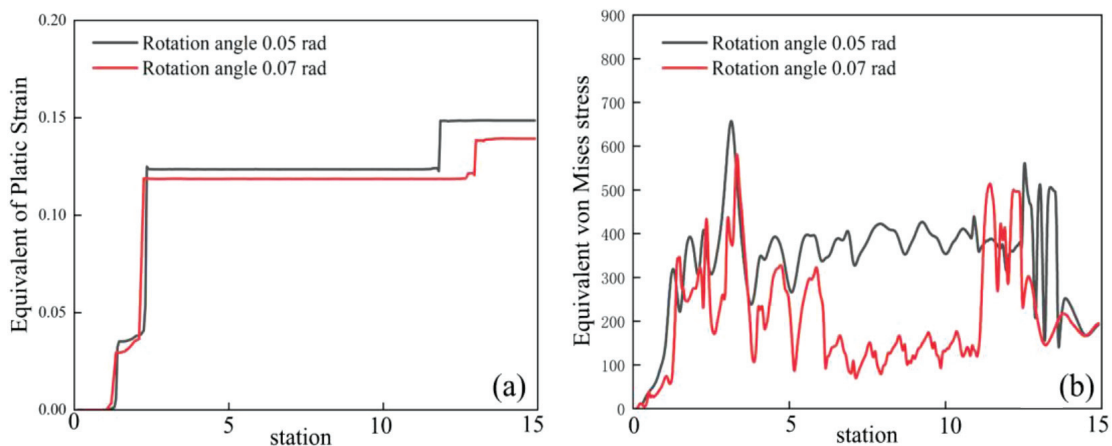


Figure 12: a) Strain and b) stress curves for two rotation angles

Figure 13 illustrates the *S/N* ratio for different parameter levels, providing a visual representation of their impact on the maximum strain. This figure aids in identifying the optimal parameter settings that minimize the strain and maximize the process stability. The analysis reveals that the line velocity and the rotation angle are the most significant factors influencing the strain, as depicted in the *S/N* bar chart.

Furthermore, **Figure 14** supports this by showing the range analysis for these parameters, directly correlating the calculated *S/N* ratios with observed strain values. The range values in **Table 4** complement this visual data, indicating each parameter's degree of influence on the forming process.

Through the combined use of Equations (2) and (3), along with graphical representations in **Figures 13** and **14**, this study provides a comprehensive understanding of how each parameter affects the process outcome. The correlation between theoretical calculations and experimental results underscores the importance of optimizing these parameters to improve the cold-roll forming process quality and efficiency.

Table 2: Parameters and their respective levels.

Parameter	Level 1	Level 2
Friction coefficient (A)	0.05	0.08
Line velocity (B)	3	10
Rotation angle (C)	0.05	0.07

Table 3: Standard orthogonal array for the experiments and results

Experiments	A	B	C	Maximum strain (%)	<i>S/N</i>
1	0.05	3	0.05	0.0352	38.1000
2	0.05	3	0.07	0.0776	31.2336
3	0.05	10	0.05	0.1485	25.5963
4	0.05	10	0.07	0.1919	23.3694
5	0.08	10	0.05	0.1119	28.0543
6	0.08	3	0.07	0.1307	26.7053
7	0.08	10	0.07	0.0966	29.3313
8	0.08	3	0.05	0.0710	32.0057

Table 4: The result of a range

Results	A	B	C
K1	0.4532	0.3145	0.3666
K2	0.4102	0.5489	0.4968
K1	0.2266	0.15725	0.1833
K2	0.2051	0.27445	0.2484
R	0.0215	0.1172	0.0651

In this study the impact of line velocity and rotation angle on the maximum longitudinal strain shows a positive correlation. In contrast, the impact of the friction coefficient shows a negative correlation. The calculated positive correlation coefficients are 0.1172, and the negative correlation coefficients are 0.0215 and 0.0651, respectively. These data indicate a high level of linear correlation between the study data. However, the relation-

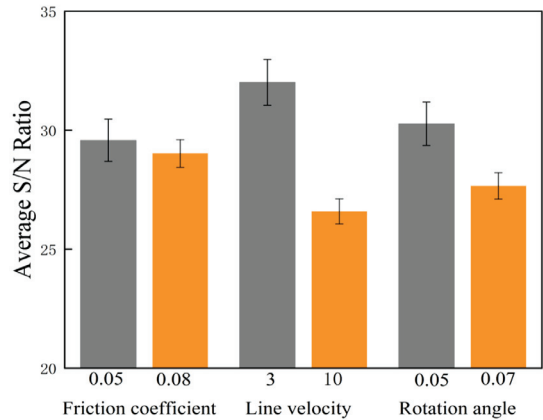


Figure 13: *S/N* under varying parameter

ship between spacing and strain is not linear, suggesting that increased depth and wider distances may hurt the strain. As the contact area between the workpiece and mold expands, the friction correspondingly intensifies, thus stimulating workpiece progression and inducing internal tension that bolsters molding stability. This enlargement of the contact area further facilitates the workpiece advancement; nevertheless, heightened friction may detrimentally impact the surface quality by inducing abrasions, smearing, and other defects. To ensure optimal surface quality in practical production settings, strategies such as lubricant application and surface coatings are implemented to alleviate frictional effects. Line velocity exerts the most significant influence on strain development; an increase in line velocity escalates strain levels, resulting in side wave formation and uneven plate surfaces. Conversely, the rotation angle exerts minimal influence on this strain. In terms of forming quality, a smaller strain indicates a better forming quality, meaning a larger average signal-to-noise ratio is preferable. The largest average signal-to-noise ratio in **Figure 12** indicates the best parameters.

Therefore, the best parameter combination can be determined through a comprehensive analysis of **Figures 13** and **14**. According to the analysis, the friction

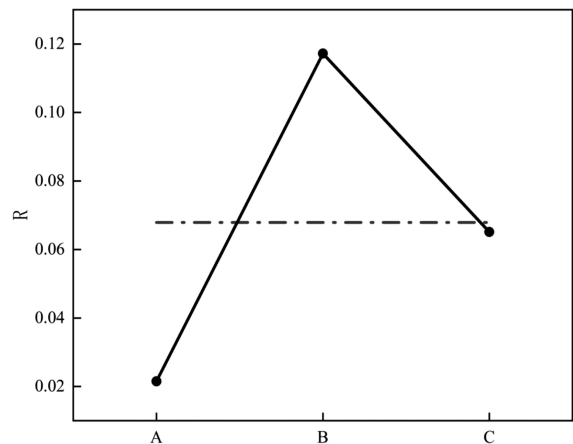


Figure 14: Value of R with 3 parameters



Figure 15: Production line of roll-forming process

coefficient is 0.05, the line velocity is 3 min^{-1} , and the rotation angle is 0.05. Numerical studies show that the equipment of the cold-roll forming production line, as illustrated in **Figure 15**, can meet the requirements for precision and surface quality. **Figure 16** shows the final products of the metal strip. These comprehensive analyses and comparisons provide strong data support for optimizing the cold-roll forming process.

5 CONCLUSIONS

This paper meticulously designed rolls using the COPRA roll-design software and simulated the roll-forming process of spiral corrugated steel tubes using finite-element modeling software. A comprehensive exploration was conducted on the impact of various process parameters on the formation of spiral corrugated steel tubes. Through carefully designed comparative and orthogonal experiments, this study further assessed the specific effects of various process parameters on the forming quality of spiral corrugated steel tubes, thus providing a solid theoretical foundation for the efficient production of spiral corrugated steel tubes. The main conclusions can be summarized as follows:

(1) The cold-roll forming process of helical corrugated tubes has shown that the line velocity and friction coefficient have a significant impact on the longitudinal strain of the sheet-metal edges. Specifically, an increase in the friction coefficient from 0.05 to 0.08 resulted in a 35 % decrease in longitudinal strain at the edges. Conversely, an increase in line velocity from 3 min^{-1} to 10 min^{-1} led to a 45 % increase in the longitudinal strain. The rotation angle, ranging from 0.01 rad to 0.05 rad, had only minimal effect on the strain, with changes limited to within 2 %.

(2) Optimization Using Orthogonal Experimental Method: The study utilized the $L8(2^7)$ orthogonal experiment method to systematically investigate and determine the optimal combination of process parameters. The optimal parameter combination for minimizing the maximum longitudinal strain includes a friction coefficient of 0.05, a line velocity of 3 min^{-1} , and a rotation angle of 0.05 rad. This result has importance for enhancing production efficiency and product quality.



Figure 16: Final products of metal strip

(3) According to the optimized process plan, the accuracy of the design was verified through production debugging and experimental validation. The validation process comprehensively evaluated the samples against key quality indicators, including dimensional accuracy, surface integrity, and structural consistency. All samples met the expected standards, with size deviations within $\pm 1.2 \text{ mm}$ (compared to the industry standard of $\pm 2.0 \text{ mm}$), indicating that the optimized parameters significantly improved the accuracy of the roll-formed products. These concrete results confirm the reliability of the optimized design, strongly support the research conclusions, and underscore its practicality in enhancing production efficiency and product quality.

Author Contributions

WanJun Chen: Methodology, Investigation, Data curation, Writing – original draft. YiYing Zhou: Data curation. Huamin Liu: Conceptualization, Data curation, Writing – review & editing.

Funding

This research received no external funding.

Institutional Review Board Statement

Not applicable.

Informed Consent Statement

Not applicable.

Data Availability Statement

The datasets used or analyzed during the current study are available from the corresponding author on reasonable request.

Acknowledgments

The authors express their gratitude to the Data M that provided the software COPRA. The authors acknowl-

edge to all the authors who contributed to this article and the teachers who provided the test analysis.

Conflicts of Interest

The authors declare no conflict of interest.

6 REFERENCES

- ¹ G. Nefussi, L. Proslie, P. Gilormini, *Journal of Materials Processing Technology*, 95 (1999) 216–221
- ² Y. Li, X. Han, J. C. Liang, F. Teng, C. Liang, *International Journal of Advanced Manufacturing Technology*, 112 (2021) 897–905, doi:10.1007/s00170-020-06574-5
- ³ J. J. Cheng, J. G. Cao, Q. F. Zhao, J. Liu, N. Yu, R. G. Zhao, *International Journal of Advanced Manufacturing Technology*, 107 (2020) 1793–1804, doi:10.1007/s00170-020-05194-3
- ⁴ Y. Fang, Y. Y. Wang, C. Hou, B. Lu, *Thin-Walled Structures*, 157 (2020) 16, doi:10.1016/j.tws.2020.107058
- ⁵ L. Yang, R. Jiang, Y. Fang, Y. Wang, *Journal of Constructional Steel Research*, 212 (2024), doi:10.1016/j.jcsr.2023.107824
- ⁶ A. Poursafar, S. Saberi, R. Tarkesh, M. Vahabi, J. J. Fesharaki, *International Journal on Interactive Design and Manufacturing (IJIDeM)*, 16 (2022) 531–543, doi:10.1007/s12008-022-00852-1
- ⁷ Y. Wang, Z. A. Mehari, J. Wu, J. Han, *The International Journal of Advanced Manufacturing Technology*, 123 (2022) 527–542, doi:10.1007/s00170-022-08155-9
- ⁸ K. S. Tsang, W. Ion, P. Blackwell, M. English: Validation of a finite element model of the cold roll forming process on the basis of 3D geometric accuracy, *Proc. of the International Conference on the Technology of Plasticity (ICTP)*, vol 207, Elsevier Science Bv, Cambridge, ENGLAND, 2017, 1290-1295
- ⁹ C. Chen, J. Liang, F. Teng, Y. Li, C. Liang, *The International Journal of Advanced Manufacturing Technology*, 112 (2020) 563–575, doi:10.1007/s00170-020-06423-7
- ¹⁰ Q.V. Bui, J.P. Ponthot, *Journal of Materials Processing Technology*, 202 (2008) 275–282, doi:10.1016/j.jmatprotec.2007.09.053
- ¹¹ X. Chen, Q. Chang, J. Wang, C. Chen, *International Journal of Modelling, Identification and Control*, 7 (2009) 97–102, doi:10.1504/IJMIC.2009.023262
- ¹² D.-S. Shim, J.-Y. Son, E.-M. Lee, G.-Y. Baek, *International Journal of Material Forming*, 10 (2016) 581–596, doi:10.1007/s12289-016-1297-1
- ¹³ M. Salmani Tehrani, H. Moslemi Naeini, P. Hartley, H. Khademizadeh, *Journal of Materials Processing Technology*, 177 (2006) 617–620, doi:10.1016/j.jmatprotec.2006.04.111
- ¹⁴ S. Maeda, *Progress in Organic Coatings*, 28 (1996) 227–238, doi:10.1016/0300-9440(96)00504-1
- ¹⁵ G. Nefussi, P. Gilormini, *International Journal of Mechanical Sciences*, 35 (1993) 867–878, doi:10.1016/0020-7403(93)90017-4
- ¹⁶ G. Nefussi, L. Proslie, P. Gilormini, *International Journal of Mechanical Sciences*, 40 (1998) 15–25, doi:10.1016/S0020-7403(98)00011-4
- ¹⁷ M. Brunet, B. Lay, P. Pol, *Journal of Materials Processing Technology*, 60 (1996) 209–214, doi:10.1016/0924-0136(96)02234-2
- ¹⁸ R. Senanayake, I. Cole, S. Thiruvarduchelvan, *Journal of Materials Processing Technology*, 45 (1994) 155–160, doi:10.1016/0924-0136(94)90093-0
- ¹⁹ H. W. Zheng, S. H. Xiang, L. Chang, Study on Production Technique of the Metal Reinforced Polyethylene Spiral Corrugated Pipe, *Proc. of the 2nd International Conference on Chemical, Material and Metallurgical Engineering (ICCMME 2012)*, vol 634–638, Trans Tech Publications Ltd, Kunming, PEOPLES R CHINA, 2012, 2040–2043
- ²⁰ A. Z. Dellil, *Mechanika*, (2014) 42–48, doi:10.5755/j01.mech.20.1.6614, 15.03.2022
- ²¹ V. A. Osadchii, S. M. Gorbatyuk, D. I. Filippov, N. S. Kuprienko, *Metallurgist*, 60 (2017) 1130–1134, doi:10.1007/s11015-017-0539-2
- ²² G. Chatzopoulou, G. C. Sarvanis, C. I. Papadaki, S. A. Karamanos: The Effect of Spiral Cold-Bending Manufacturing Process on Pipeline Mechanical Behavior, *Proc. of the 11th International Pipeline Conference (IPC 2016)*, Amer Soc Mechanical Engineers, Calgary, CANADA, 2016
- ²³ J. Wang, H.-M. Liu, S.-F. Li, W.-J. Chen, *Materials*, 15 (2022) 8023, doi:10.3390/ma15178023, 30.01.2023
- ²⁴ C. Liang, S. Li, J. Liang, J. Li, *Metals*, 12 (2021) 53, doi:10.3390/met12010053.
- ²⁵ Y. Wang, X. Xu, H. Liu, J. Liu, R. Zhao, *ACS omega*, 7 (2022) 4804–4811, doi:10.1021/acsomega.1c05356